Numerical analysis of progressive damage in nonwoven fibrous networks under tension

Farukh Farukh [(1)], Emrah Demirci [(1)], Baris Sabuncouglu [(1)], Memiş Acar [(1)], Behnam Pourdeyhimi [(2)], *Vadim V. Silberschmidt [(1)]

1 - Wolfson School of Mechanical and Manufacturing Engineering, Loughborough University, UK

2 - Nonwovens Cooperative Research Center, North Carolina State University, Raleigh, NC, USA

*Corresponding author's e-mail: V.Silberschmidt@lboro.ac.uk

Tell: +441509227504; fax: +441509227502

Add.: Wolfson School of Mechanical and Manufacturing Engineering, Loughborough University, UK

Keywords: non-woven fabrics; damage; microstructures; failure; finite element

Abstract:

Understanding a mechanical behaviour of polymer-based nonwoven materials that include large-strain deformation and damage can help to evaluate a response of nonwoven fibrous networks to various loading conditions. Here, a nonwoven felt made by thermal bonding of polypropylene fibres was used as a model system. Its deformation and damage behaviour was analysed by means of experimental assessment of damage evolution based on single-fibre failure and finite element simulations. Tensile tests of nonwoven fabrics were carried out to characterise their damage behaviour under in-plane mechanical loading. It was found that progressive failure of fibres led to localization of damage initiation and propagation, ultimately resulting in failure of the nonwoven felt. To obtain the criteria that control the onset and propagation of damage in these materials, tensile tests on single fibres, extracted from the felt with bond points attached to their ends, were performed. A finite-element model was developed to study damage initiation and propagation in nonwovens. In the model, structural randomness of a nonwoven fibrous network was implemented by means of direct introduction of fibres according to the orientation distribution function. The evolution of damage in the network was controlled by a single-fibre failure criterion obtained experimentally. The proposed numerical model not only captured the macroscopic response of the

felt successfully but also reproduced the underlying mechanisms involved in deformation and damage of nonwovens.

1. Introduction

Nonwoven fibrous networks demonstrate complex deformation and damage behaviour linked to randomness of their microstructure and properties of constituent fibres. In thermally bonded calendered nonwovens, a fabric's structure is composed of continuous and discontinuous regions. These continuous regions called *bond points* are connected by a network of randomly oriented fibres forming a discontinuous region with voids and gaps in it. This combination of two regions with different microstructures, with continuous domains embedded into discontinuous medium, makes it difficult to predict the deformation and damage behaviour of thermally bonded fibrous networks. Experimental characterisation is not always viable and sufficient for a comprehensive understanding of complex phenomena involved in deformation and damage of nonwoven fibrous mats. The challenges involved in experimentation are linked to the need for specialised experimental devices as well as to significant efforts required for experimentation, especially for this type of materials, in which mechanical properties are defined by their non-trivial microstructure and constituent fibres' properties. To tailor and optimise properties of these materials, an understanding of the relationship between their macroscopic behaviour and microstructure along with manufacturing-defined single-fibre properties is essential. Therefore, the aim of this work is to develop a numerical model incorporating the fabric's microstructure, properties of constituent fibres and main deformation and damage mechanisms.

The behaviour of woven fibrous networks that are mostly used in composites for various multi-functional applications, is better understood than that of nonwoven fibrous networks (either as standalone fabrics or in combination with epoxies in the form of composites) (Li *et al.*, 2010; Blacklock *et al.*, 2012; Rinalidi *et al.*, 2012; Parsons *et al.*, 2013). Still, several studies were performed to model and predict the mechanical response of nonwoven fibrous networks. Most of

the work in this field is related to paper, which is a very special type of nonwoven (Schulgasser, 1981; Ostoja-Starzewski *et al.*, 2000; Isaksson and Hagglund., 2004; Isaksson *et al.*, 2007; Isaksson and Hagglund., 2009; Harrysson *et al.*, 2008; Bronkhorst, 2003). In the context of nonwoven networks, several techniques were used to simulate a mechanical behaviour of these materials. A continuum model incorporating an orientation distribution of fibres by considering orthotropic symmetric planes was developed (Demirci *et al.*, 2011, 2012). This model was used successfully to predict the stress—strain behaviour of high-density nonwovens but it was incapable to account for changes in the network's topology with localization of damage. Ridruejo *et al.* (2012) introduced a continuum model to predict a meso-level response of the fabric without explicit introduction of fibres into the model, and thus, it was unable to reproduce the effect of the actual microstructure; mechanisms of fabric's deformation and damage were implemented in a phenomenological way. In order to resolve the issues with continuum models, another technique based on a composite laminate model, incorporating the effect of non-uniform orientation distribution of fibres, was used (Singh *et al.*, 1998). In that model, fibre layers were stacked on top of each other in a way that the fibres in each new layer were at an angle relative to that in the preceding one. This model was unable to capture all the aspects of the real fabric's behaviour such as re-orientation of fibres since they were fixed within the layer and could not slide on top of each other. In an effort to incorporate a realistic non-uniform microstructure of nonwovens into the model, an approach based on homogenization was developed using a representative volume element (RVE). Petterson (1959) introduced the model to predict a macroscopic response of the fabric by homogenizing the behaviour of a unit cell incorporating a random distribution of fibres' orientation. More recently, Silberstein *et al.* (2012) suggested an approach of employing a similar RVE-based technique to predict a macroscopic behaviour of the fabric. The model consists of a multilayer triangular network and uses a homogenization technique to predict a response to monotonic and cyclic loading. Such models based on the homogenization technique do not predict localization of damage and changes in material's microstructure caused by this damage. In order to overcome these

shortcomings, microstructure-based models employing direct introduction of individual fibres according to their orientation distribution were developed (Hou *et al.*, 2009, 2011a, 2011b; Sabuncouglu *et al.*, 2012a; Farukh *et al.*, 2012a). Though this modelling technique is computationally not as efficient as a continuum one, however, it can account explicitly for all the main mechanisms involved in deformation and fracture of nonwovens. Moreover, a model based on this technique naturally introduces voids and gaps into consideration that are a distinctive feature of fibrous networks especially in case of low-density nonwovens. Such models can simulate the deformation behaviour of the fabric very accurately but up to a certain level of deformation; none of these models can predict the damage initiation and propagation in nonwovens. A model, based on the same approach to introduction of discontinuous microstructure, was presented by Ridruejo *et al.* (2011) who employed bundles of random fibres, without using their actual orientation in the real fabric, in the model. With that approach, a glass-fibre nonwoven felt, in which damage of the fabric occurred as failure of bonds rather than fibre bundles, was studied. In addition to these, models have been proposed by Isaksson *et al.* (2012) and Wilbrink *et al.* (2013) focussed on a crack-growth direction and bond failure in fibrous networks, respectively. Thus, it can be concluded that despite of the benefits of different reviewed models for analysis of various aspects of mechanical behaviour and mechanisms involved in deformation and failure of nonwoven fibrous networks, they present only partial solutions. None of the models can predict evolution of deformation and damage of the fabric up to its failure in terms of progressive failure of fibres while incorporating explicitly the realistic material's microstructure by introducing fibres and constituent fibre properties into the model.

In this paper, a thermally bonded nonwoven fibrous network with its actual microstructure was modelled in finite-element environment using a parametric modelling technique based on a specially developed user subroutine. A random anisotropic nature of the fabric was captured by introducing the fibres directly into the model according to their orientation distribution in the fabric. The variability of elastic-plastic mechanical properties of constituent fibres and a single-fibre failure

criterion were introduced into the model. Damage initiation and evolution in the model were controlled by this criterion as progressive failure of fibres resulted in damage initiation and propagation in nonwovens.

2. Experimentation

The model developed in this paper is based on experiments with single fibres and a nonwoven fabric reported in (Farukh *et al.*, 2012b). These experiments provided information necessary for development of a finite-element model, such as a number of fibres and their orientation distribution function, dimensions of bond points, their shape, and a pattern obtained from morphological characterisation of the fabric as well as material properties obtained in single-fibre experiments. Moreover, tensile tests performed on specimens of the fabric provided a basis for physical interpretations of the results obtained with the model not only in terms of material's constitutive behaviour but also the mechanisms involved in its deformation and damage. Therefore, single-fibre and fabric experiments crucial for this study are briefly recalled here.

2.1 Material

The materials used in this study were low-density (< 50 g/m^2) thermally bonded calendered nonwovens based on polypropylene (PP) fibres, manufactured by FibreVisions®, USA. Polypropylene fibres of 18 µm diameter were used to manufacture a fabric. The staple fibre with length of 38.1 mm were laid randomly on a conveyor belt resulting in an anisotropic web, in which more fibres were oriented along the direction of the belt, called *machine direction* (MD) as compared to that in the direction perpendicular to MD on the plane of the web, called *cross direction* (CD). The web was then bonded with a hot calendering technique at a temperature of 156^{o}C, which lies within the optimal temperature window for PP. Different basis weights of material, i.e. 20, 30 and 40 g/m^2 were used in this study. The overall microstructure of the fabric is shown at different scales in Fig. 1.

2.2 Assessment of properties

2.2.1 Single-fibre behaviour

The material properties, especially related to failure, of single fibres extracted from the studied thermally bonded fabric are different from those of the virgin fibres due to the pressure and temperature involved in the bonding process (Chidambram *et al.*, 2000; Wang and Michielsen, 2001; Michielsen and Wand, 2002; Wang and Michielsen, 2002; Bhat *et al*, 2004; Farukh *et al.*, 2012b). Therefore, individual fibres extracted from the fabric were used to obtain their material properties as these are its basic constituent. A complete detail on fibre extraction and preparation of the specimen is given in (Farukh *et al.*, 2012b). Tensile tests were carried out on those extracted fibres at various levels of constant engineering strain rates — 0.5, 0.1 and 0.01 1/s — using Instron® Micro Tester 5848 with a high-precision ±5 N load cell. Due to difficulties to control the fibre's length, a constant engineering strain rate was achieved by modifying the velocity of the cross-head with respect to the length of each fibre specimen. The following relationship was used for this purpose:

$$\frac{\nu}{l_o} = \dot{\varepsilon} = \text{const}, \tag{1}$$

where v is the cross-head velocity and l_o is the initial length of the fibre. In order to assess variability of the obtained results, at least ten samples were tested for each strain rate. True strains ($\varepsilon_{\text{true}}$) and true stresses ($\sigma_{\text{true}}$) were recorded during the tests:

$$\varepsilon_{\text{true}} = \int_{l_o}^{l} \frac{dl}{l} = \ln\left(\frac{l}{l_o}\right), \tag{2}$$

$$\sigma_{\text{true}} = \frac{F(1+\varepsilon_{\text{eng}})}{A_o}, \tag{3}$$

where l is the current specimen length, F is the load, A_o is the initial area of fibre's cross-section and ε_{eng} is engineering strain. In these calculations, it was assumed that the fibre's cross-section was

perfectly circular and its diameter was constant along its length. True stress and true strain were computed based on the hypothesis that deformation in fibre took place at constant volume. The true stress-true strain curves obtained from the tests had a sigmoidal shape with elastic-plastic region (Fig. 2). The values of material density (ρ_f), elastic modulus (E_f), Poisson's ratio (ν_f) and initial yield stress (σ_y) are given in Table 1. The tested fibres showed a scatter in results along with variation in their stress-strain behaviour with a strain rate, which is due to viscous properties of the material. The elastic-plastic properties obtained from the single-fibre tensile tests were used as input into the finite-element model.

2.2.2 Microstructural characterisation

Characterisation of microstructural features of the undeformed network (fabric) was performed using scanning electron microscopy (SEM) (Carl Zeiss, Leo, 1530VP FEGSEM). One of the typical images obtained with SEM is shown in Fig. 1a. Dimensions of structural entities such as bond points and their pattern as well as orientation distribution of fibres required for the development of the finite-element model were obtained from these images. The complete details of determining the orientation distribution function (ODF) of fibres using an in-house software Nonwoven Anisotropy V1 were given in (Farukh *et al.* 2012a). The ODF obtained from these experiments is presented as a histogram in Fig. 3, which shows preferential orientation of fibres in MD as compared to CD and, thus, quantifies anisotropy of the studied fabric.

2.2.3 Mechanical behaviour

Rectangular coupons along the machine direction and cross direction were cut from the studied nonwoven fabric with the basis weight of 20 g/m^2, and uniaxial tensile tests were performed on these specimens at strain rate of 0.1 and 0.01 1/s using Hounsfield Benchtop Tester with pneumatic grips. The force-extension graphs obtained from these experiments for both MD and CD direction are given in Fig. 4. These experiments demonstrated not only differences in the mechanical behaviour of the fabric in MD and CD but a significant scatter in results for both directions due to

the irregularities in fabric's microstructure as well as geometric and material properties of constituent fibres. Along MD, the maximum load was attained at lower fabric's extension as compared to that in CD followed by a gradual process of fibre failure giving the bell-shaped form to the force-extension curve. In contrast, a rapid fibre-failure process following large fabric's extension was observed in CD resulting in a sudden drop on the force-extension curve. The features presented by the curves for various specimens in any particular direction — MD or CD — were the same, shown by solid lines in Fig. 4, even with a significant scatter among them. These lines correspond to experimental results giving the approximately median values of force and extension. The difference in load-carrying capacity of the material in MD and CD ascertain the anisotropic nature of the fabric.

In order to study microstructural features of the deformed fabric, a high-speed camera (Photron Fastcam SA3) with advanced macro capabilities was used. Large rotations of fibres towards the loading direction followed by their progressive failure when they reached their stress or strain threshold were observed in these tests. The progressive failure of fibres was associated with the development and growth of localized fracture zones, formed by remaining fibres aligned along the loading direction, leading ultimately to failure of the fabric specimen; the sequence of these phenomena is shown in Fig. 5. When these experiments were repeated on fabrics with different basis weights, it was observed that the main mechanisms involved in deformation and damage of those materials remained the same. Furthermore, the strain rate did not cause any effect on the sequence of deformation and damage phenomena. These observations were close to those presented by Ridruejo *et al.* (2011).

The phenomena of deformation as well as damage initiation and progression were effectively the same for both MD and CD except for the fact that rotation of fibres before their full engagement in load transfer was rather large in CD as compared to that in MD; this was due to the preferential orientation of fibres along MD. Moreover, this orientation resulted in a significantly higher load-

bearing capacity in MD than CD apparent in Fig. 4. During deformation and damage of nonwovens, only rotation of bond points was observed, without any significant deformation of them. However, they played an important role in progressive failure of fabric as fibres always break at bond-point periphery.

2.2.4 Damage analysis

Damage in the studied thermally bonded nonwovens was initiated by failure of fibres reaching their stress or strain thresholds during the loading. This triggered the development of fracture zones within the fabric growing with subsequent fibre failures. This growth of fracture zones due to progressive failure of fibres ultimately led to rupture of the fabric. In thermally calendered bonded nonwovens, most of the fibres fail at the bond periphery in well-bonded and over-bonded fabrics due to the effect of manufacturing processes (Chidambram *et al.*, 2000; Michielsen and Wand, 2002; Wang and Michielsen, 2002; Bhat *et al*, 2004). During manufacturing of thermally bonded nonwovens, fibres in areas of bond points melt partially due to high temperature and pressure involved and join together at a cooling stage. The bonding process results in changes in molecular orientation of fibres forming the bonds. The change in microstructure is rapid near the bond periphery leading to a decrease in the elastic modulus and strength of the fibres at bond edge (Chidambram *et al.*, 2000; Wang and Michielsen, 2001; Michielsen and Wand, 2002; Wang and Michielsen, 2002; Bhat *et al.*, 2004). Another obvious reason is a stress concentration at the fibre-bond point interface. As a result, it is not possible to use the material properties of virgin fibres or even of processed ones without taking the bond-point periphery region into account in damage analysis of the fabric. Thus, in this study, fibre samples were extracted from the fabric in a way that they were attached to individual bond points at their ends. Sticky strips of paper were attached to the bond point at the edges of the fibre for firm grip during testing. The strips were attached to the bond points as close to their edge towards the fibre as possible. That allowed the accurate stress-strain behaviour of the processed fibre to be obtained without amalgamating it with that of the bonds. Uniaxial tensile tests at strain rate of 0.01, 0.1 and 0.5 1/s were performed on these samples to obtain the failure parameters, i.e. ultimate

tensile stress and corresponding strain. The same tests were performed on raw PP fibres used for manufacturing of the analysed nonwoven; it was found that failure stress and corresponding strain of fibres in thermally bonded nonwovens were significantly lower than those of the unprocessed fibres as shown in Fig. 6. The experiments did not provide constant levels of failure strength and strain-at-failure; rather, there was a significant scatter in the obtained results. In order to assess the variability of results, tensile tests at each strain rate for processed and unprocessed fibres were repeated for at least ten times. Since damage initiation and propagation in nonwovens is associated with progressive failure of fibres, the experiments of single fibres with bond points at their edges provided the damage criteria necessary for modelling of deformation and damage behaviour of nonwovens.

3. Modelling of nonwoven fabric

3.1. Generation of fibrous network

In case of fibrous networks, their randomness as well as presence of voids and gaps in their microstructure necessitates development of the model incorporating a realistic orientation distribution of fibres in the fabric. The finite-element technique offers an opportunity to develop a numerical model based on the mechanical behaviour of constituent fibres and microstructure of the network, which could predict the deformation and damage behaviour in nonwovens.

A FE model of the studied nonwoven material was developed within the MSC. Marc software package using MSC. Patran as pre-processor. Starting from the material's microstructure, the finite-element model was developed with the help of a subroutine, written in Patran Command Language (PCL), employing a parametric modelling technique as mentioned in (Sabuncuoglu *et al.*, 2012, 2013; Farukh *et al.*, 2012a). In the model, the anisotropic nature of the fabric microstructure was introduced by modelling the fibres directly according to their orientation distribution in the fabric. Modelling of fibres according to their determined ODF (Fig. 3) was performed using the subroutine that incorporates a realistic microstructure of the fabric into the model. The FE model of the fabric developed in this study consists of bond points connected by the linking fibres. The bond points were modelled with shell elements (element type 139 in

MSC. Marc) with thickness identical to those in the fabric. The chosen finite element is a four-node, thin-shell element with global displacements and rotations as degrees of freedoms; a bilinear interpolation is used for the displacements and rotations. All the constitutive relations including a viscoelastic-plastic one can be used with this element. Because of these attributes, element 139 is suitable for representation of bond points and used in our simulations. It is defined geometrically by (x, y) coordinates of its four corner nodes. Due to the bilinear interpolation, the surface forms a hyperbolic paraboloid, which is allowed to degenerate to a plate. The shell elements are suitable to simulate the bond points in this study with a high edge-length-to-thickness ratio. Besides, they provide the opportunity to extend the use of the developed FE model to out-of-plane loading regimes (published elsewhere).

Fibres were modelled with truss elements (element type 9 in MSC. Marc), which have only axial stiffness. Since truss elements cannot carry any bending moment, they were appropriate for representation of fibres characterised by a rather low flexural stiffness. The chosen element type for fibres can describe properly a high level of deformations, characteristic to this type of nonwovens, as well as stress stiffening. This was verified by performing FE simulations of a case study for a single-fibre experiment before implementing the full numerical model. The total numbers of both types of elements for MD and CD models are given in Table 2. Information about the size, shape and pattern of bond points was obtained from SEM images of the fabric (see Table 3 and Fig. 7). In order to introduce the real material properties into the model, it is essential to determine the number of fibres to be modelled. This is calculated by the following relation:

$$N_{\text{Fibre}} = \frac{L_{\text{Fibre}}\ \rho_{\text{Fibre}}\ a_{\text{Fibre}}}{\rho_{\text{Fabric}}\ A_{\text{Fabric}}\ k}, \tag{4}$$

where L_{Fibre} is the length of single fibre, ρ_{Fibre} is the density of constituent fibre material, a_{Fibre} is the fibre's cross-sectional area, ρ_{Fabric} is the areal density of the fabric, A_{Fabric} is the area of the fabric with dimensions equal to those of the FE model and k is the model coefficient equal to a number of

fibres represented by a single truss element in the model. The value of k can be changed from 1 to a higher magnitudes depending upon the efficiency of the computational system. If $k = 1$, each truss element represents the behaviour of a single fibre, and the number of truss elements introduced into the model is exactly equal to the number of fibres in the fabric's sample with dimensions equal to those of the FE model. If the efficiency of the computational system is low and a higher value of the model coefficient k is used, the geometric properties related to fibre should be updated respectively. For example, if $k = 4$ is used, the diameter of the truss element should be two times the diameter of a single fibre. Using the input information about the parameters mentioned in Eq. (4), the subroutine facilitates calculation of the number of fibres and introduction of truss elements into the model according to the ODF into the model. Since this model is based on the parametric modelling technique, it can be easily reformulated for different realizations of orientation distribution of fibres, sizes, shapes and patterns of bond points as well as fabric dimensions and areal densities. The developed network geometry for 20 g/m^2 fabric is shown in Fig. 9a.

3.2. Finite-element model

The generated fibrous network was discretised into finite elements. Each truss element between the bond points was considered as one element. After spatially random distribution of fibres, based on the measured ODF, the location of respective truss elements was slightly adjusted to obtain the regular mesh in the bond points and to ensure connectivity between the truss and shell elements. In order to do this, the shell element was divided virtually into equal pieces, each with dimensions of the mesh element. Then, the tip of each fibre (the node of the truss element) attached to this bond point was shifted, if necessary, to the closest node of the shell elements on the exterior of the domain representing the bond point. Thus, a regular mesh in bond point was achieved with proper connectivity of truss elements (fibres) with shell elements (bond points). The mesh and connectivity of truss elements with shell elements is shown in Fig. 9b. The complete details of this process as well as of a generation of the parametric model are published elsewhere (Sabuncouglu *et al*., 2012, 2013). As mentioned earlier, in experiments, during fabric's extension most fibres reorient

themselves along the direction of stretching and undergo tensile loads. As a result, the number of fibres under compressive load is almost negligible as compared to that under tensile load. In order to simulate the global deformation of nonwovens, the local behaviour of the bulk of the fibres (under tension) must be properly accounted in simulations. Hence, to predict the behaviour of nonwoven accurately, truss elements were chosen to model fibres as they carry negligible bending load similar to real fibres in the network. Still, some of the truss elements carry compressive load depending upon their orientation distribution in the nonwoven structure (similar to real fabric, in which some of the fibres buckle under compressive loading) but that contributes very little to the global behaviour of the fabric.

The influence of single-fibre material properties on the mechanical behaviour of the nonwoven network was incorporated by assuming fibres as isotropic, elastic-plastic with piece-wise linear hardening. The total strain of the fibre was a combination of elastic and plastic contributions. In the elastic region, stresses in the fibres as a function of strain can be obtained by relating these two using the elastic modulus, whereas the von Mises yield criterion was used for the onset of plastic deformation. Since fibres are explicitly introduced into the model as truss elements that bear only axial load, the von Mises yield criterion reduces simply to $\sigma_1 = \sigma_y$, meaning that fibres start yielding when the stress level in them reaches their corresponding yield strengths. The latter were obtained from single-fibre uniaxial tensile tests performed in this study. Thus, the incremental stress-strain relation in fibres in elastic region is given as (Simo and Hughes, 1997; MSC. Marc, 2013):

$$\sigma_e^{n+1} = \sigma_e^n + E\Delta\varepsilon_e^{n+1}, \tag{5}$$

where E is the Young's modulus. Using the flow stress definition based on table-based input, the hardening slope at each increment is obtained by numerically differentiating the values given in the

table; these values are based on a plot of the stress versus plastic strain for a tensile test. The generalized form of the work-hardening coefficient has the following form:

$$H = \frac{d\bar{\sigma}}{d\bar{\varepsilon}^{\mathrm{p}}}, \tag{6}$$

where $d\bar{\varepsilon}^{\mathrm{p}}$ and $d\bar{\sigma}$ are equivalent plastic strain and equivalent stress. The flow rule, describing changes in plastic strain component as a function of the current stress state), essential to define the incremental stress-strain relation for plastic material, can be expressed as:

$$d\varepsilon^{\mathrm{p}} = d\bar{\varepsilon}^{\mathrm{p}} : \nabla\bar{\sigma} \quad \text{where} \quad \nabla\bar{\sigma} = \frac{\partial\bar{\sigma}}{\partial\sigma_{\mathrm{ij}}}. \tag{7}$$

It can be shown (MSC. Marc, 2013) that By rearrangement

$$d\bar{\varepsilon}^{\mathrm{p}} = \frac{\nabla\bar{\sigma} : C : d\varepsilon}{H + \nabla\bar{\sigma} : C : \nabla\bar{\sigma}}, \tag{8}$$

where C is the stiffness matrix.

3.3. Material properties and boundary conditions

The material properties implemented into the model were obtained from the single-fibre tensile tests. The experimental curves of single-fibre tensile tests (Fig. 8a) were used to define the elastic-plastic behaviour of the fibres in the developed model. It was found that there was a significant scatter in results of single-fibre experiment results (Fig. 8a), which show the randomness in material properties of the constituent fibres. This scatter was the result of some local shape irregularities of the tested fibres due to the effect of heat or physical contact during the web-forming or hot-calendering stages. In addition to shape irregularities, SEM images of the fabric showed that a fibre diameter is not constant along its length; this is another reason for a significant scatter in the results. This scatter in single-fibre experimental results was introduced into the model; it means that different flow curves (and, respectively, yield points) were assigned to the fibres in the model based

on the experimental data. It was found that implementation of variation in fibres' material properties not only in terms of their failure parameters but also the stress-strain curves along with the fibre orientation distribution into the FE model is essential to simulate a realistic deformation and damage behaviour of the fabric (Farukh *et al.*, 2012b). Therefore, different stress-strain curves and damage parameters were assigned in a random way to the truss elements in the FE model according to the data obtained from the tensile experiments at strain rate of 0.1 1/s performed on ten processed single-fibre specimens. These data was used as an indicator of scatter in material properties for all the fibres within the fabric. According to this, seven sets of fibres with different material properties in terms of stress-strain relationships and damage parameters were implemented in the model (Fig. 8). The numbers of fibres in each set as a fraction of the overall number of fibres within the fabric, obtained with the random sampling technique, with their corresponding stress and strain threshold values are given in Fig. 8. Since damage was not observed in the bond points during the fabric's tensile tests, therefore, damage criteria discussed below were not applied to them. The simulations of tensile tests were carried out by applying a set of boundary conditions to the FE model, within the framework of the implicit algorithm for quasi-static loading with large displacements and rotations. The FE solver (MSC.Marc) in this study is based on the total Lagrangian method, using the second Piola-Kirchhoff stress and Green-Lagrange strain (the details can be found in (MSC.Marc, 2013)). The nodes on the side R-S of the model (Fig. 9) were fully constrained whereas a uniform axial displacement condition corresponding to the strain rate of 0.1 1/s was applied to the nodes on side P-Q of the model as shown in Fig. 9.

3.4. Modelling of damage

Upon stretching the nonwovens, fibres start to re-orient themselves along the loading direction and increasing their participation in a load-bearing. The fibres fail when the applied stresses reach their strength threshold causing damage initiation in nonwovens. Further failure of fibres results in damage propagation followed by ultimate failure of the fabric. Since fibres are randomly oriented within the fabric and have different levels of stress and strain threshold, they fail progressively

resulting in a gradual growth of damage in nonwovens. The mechanisms involved in damage initiation and growth as well as the changes in network topology due to fibres' failure can be explicitly accounted for in the discontinuous model based on direct introduction of fibres, with their actual orientation distribution, into the model like the one developed in this study.

Numerical simulations of the onset and propagation of damage as a result of progressive failure of fibres could be taken into account using critical stress or strain-based failure criteria or the combination of both.

Since fibres are represented by two-dimensional truss elements in this study that can bear only uniaxial loads along the direction of loading, therefore, the formulation of failure criteria used in the developed model are:

Critical stress failure criterion:

$$\text{If}\left(\frac{\sigma_1}{Y_t}\right)=1,\ d_\sigma=1. \tag{14}$$

Critical strain failure criterion:

$$\text{If}\left(\frac{\varepsilon_1}{e_{yt}}\right)=1,\ d_\varepsilon=1. \tag{15}$$

Here, σ_1 and ε_1 are longitudinal stress and strain at integration point of a truss element, respectively; Y_t and e_{yt} represent maximum allowable longitudinal tensile stress and maximum allowable longitudinal tensile strain, respectively. d_σ and d_ε are the damage variables associated with the failure mode of an element under tensile stress and strain, respectively. As was observed in the tensile tests on the studied fabric at various strain rates, some of the fibres sustained their participation in load bearing even at strain levels larger than critical strain values for single fibres at

corresponding strain rates (Fig. 10a). Following these experimental observations, it was decided to use only the maximum tensile stress for the single-fibre failure in FE model; the respective values used in the FE model are given in Fig. 8. Since fibres were introduced explicitly into the model, the critical stress values of fibres obtained with the single-fibres tensile tests performed at the strain rate corresponding to model's boundary conditions were used as failure criterion in this study. In FE simulations, an element-deletion approach was used to remove the elements from the model based on the value of damage variables as calculated with Eq. (14). An element (fibre in this study) was assumed to fail and removed from the model when the damage condition (i.e. $d_\sigma = 1$) was satisfied at its integration location to avoid the convergence problem. Thus, the damage parameters were calculated for all the fibres and the elements with $d_\sigma = 1$ were removed from the model and did not offer any resistance to subsequent deformation.

4. Numerical results and discussion

The parametric computational model that captures the fabric's anisotropic behaviour linked to its microstructure and material properties of its constituent fibres was developed; it also incorporates the critical stress-based single-fibre failure criterion. This model was used to predict the behaviour of thermally bonded nonwoven. The deformation and damage behaviour in the fabric, which is a result of large rotations and progressive failure of fibres, was simulated for both MD and CD, as shown in Fig. 10b and Fig. 11b. Apparently, the main features of deformation and damage process, observed in real specimens of the modelled fabric, including formation and growth of localized zones, are reproduced in simulations. In order to compare the model's predictions with experimental results, the force-extension graphs were used as shown in Fig. 12. The shaded areas in Fig. 12 represent the bands of experimental results performed on multiple specimens for the corresponding directions. A good agreement between the simulations and experimental results was observed, including the extent of material's anisotropy. Implementing different statistical

realizations of material properties by changing them for corresponding fibre sets based on the experimentally obtained data (Fig. 8), led to changes in force-extension curve as shown in Fig. 12.

Apparently, an initial slightly stiffer behaviour in CD as compared to experiments can be attributed to the fact that a curl of fibres was not introduced into the model. This can be explained by predominant orientation of fibres along MD, with a small fraction aligned along CD. When stretched in MD, most of fibres in the fabric start participating in load-bearing early, reducing the effect of curl. Thus, the tested specimens showed an almost negligible portion of compliant behaviour in MD, whereas the fabric's subsequent response was dominated by the stretching behaviour of the fibres, which the developed model can predict rather well. However, in the specimens stretched in CD, most fibres at first reoriented along the direction of loading, with fibre curl playing an important part in this process. Hence, a significant portion of the fabric's initial response for this direction (CD) was dominated by uncurling and rotation of fibres rather than their stretching. This resulted in a compliant initial behaviour of the fabric tested in CD, which the model without the account for fibre curl could not reproduce fully adequately, predicting somewhat stiffer results.

Another apparent difference between the model's prediction and experimental results is the scatter being higher in the latter case. The experimental scatter can be related to the following factors: variation in material properties and strength of fibres, randomness in microstructure and variation in fibres' geometry. The first source of scatter was taken into account in the simulations by providing different material properties and levels of strength to different sets of fibres as shown in Fig. 13. Randomness in material's microstructure can be easily implemented into the model by using the parametric modelling technique based on the subroutine, developed in this study. In the experiments on the studied fabric, all the testing parameters such as specimen size and boundary conditions were kept constant; the variation was linked to the orientation distribution, material properties and position of fibres. Thus, it is obvious that using different microstructures by

changing the ODF for developing the model and seeding random numbers to fibre positions (Fig. 13) would increase the extent of variability in simulation results providing better agreement with the experimental results. The effect of varying the material properties of individual fibres in the form of force-extension curve is given in Fig. 12. It should be noted that the variation in the mechanical response based on assigning different material properties to fibres in the models was identical to scatter reported experimentally.

Explicit introduction of fibres into the model can help to predict the levels of stresses and strains in each element (fibre in this case) of the model. Since fibres were modelled randomly according to the ODF measured for the real fabric and their participation in load bearing changed as they were aligned along the loading direction, the level of strain (ε_f) and corresponding stress (σ_f) in each fibre varied from the global strain in the fabric ($\bar{\varepsilon}$) depending upon its orientation with respect to the loading direction and position in the network as shown in Fig. 14 and Fig. 15. The probability distribution functions of normalised strains in fibres with respect to global strain and corresponding stresses at various levels of fabric's extension are presented for each interval of strains and stresses in Fig. 14 and Fig. 15, respectively. As most of the fibres failed at levels less than 100% of fabric's extension along MD, therefore, the figures present the data for strains and corresponding stresses not exceeding this magnitude. Two different patterns of change in the probability distributions for MD and CD with increasing deformation of the fabric are obvious in Fig. 14. For CD (Fig. 14b), the distribution effectively retains its shape for different strains with only minor changes to the bands. For MD (Fig. 14a), in contrast, significant shifts of the distribution's median are observed. The peak for normalised fibre strains shifts to lower values with increasing fabric strain. The difference in patterns for stress distributions for MD and CD (Fig. 15) is also similar to that for normalised strains. Still, if for CD the character of changes is practically the same, the case of MD (Fig. 15a) has its specific development. Here, at the initial stage (up to fabric strain of 50%), the shift is to higher levels of stress of fibres, reflecting their increasing participation in the load-bearing process as a result of reorientation towards the loading

direction. However, this trend reversed between 75% and 100% of fabric's extension when many fibres reached their stress threshold and failed resulting in the stretch back of fibres outside the localised failure zones due to elasticity (Fig. 10a). Thus, the developed model can be used to predict stress distributions at any level of fabric's extension. Besides, explicit introduction of fibres into the model helped to understand the evolution in stresses in fibres and arrangement of the neighbouring elements caused by progressive failure of fibres. This demonstrates that model is also capable to qualitatively reproduce the changes in the topology of the network. Since most of the fibres regain their unstressed or low-magnitude-stress state at 100% of fabric's extension along MD (Fig. 15a), therefore, the stretch back in the fabric after 100% fabric extension is negligible as shown in Fi.g 10a (v) and (vi).

The discussed change in distributions of fibres' parameters with increasing deformation of the fabric is also reflected in changes of the maximum and minimum values of stresses shown in Fig. 16. Apparently, the maximum stress in fibres along MD and CD increased continuously until it reached its maximum value. However, this increase for MD was rapid as compared to that for CD; fibres in the former case started to participate in load bearing earlier than in the latter; this is consistent with the fabric's structure having preferential orientation of fibres along MD. The minimum value of stress in fibres for CD was negative as a result of lateral shrinking. Such fibres under compressive load offered resistance to reorientation of other fibres along the loading direction during the fabric's extension process; therefore, the model predicted a slightly stiffer behaviour compared to that observed in the experiments as shown in Fig. 12b. An interesting point can be noted here: the variation in the minimum value of stresses for both MD and CD was negligible for all the levels of fabric's extension as a result of a continuous transfer of stresses to the neighbouring elements caused by progressive failure of fibres. Due to this stress shift, some fibres start to take load during fabric's extension while some fibres return back to the unstressed state due to failure of their neighbours.

The process of reorientation of fibres towards the loading direction followed by their failure upon reaching the critical stress led to localisation of damage in the form of fracture zones as shown in Fig. 10 and Fig. 11, which appearance was similar to that observed in experiments. (A fracture zone in this study is a narrow gap in the direction of loading caused by the localized failure of fibres and formed by remaining fibres adjoining this gap.) The development of localised fracture zones was caused by an avalanche of failures due to load redistribution (i.e. increase in the load of neighbouring fibres transferred from the ruptured ones). Subsequent loading caused more fibres to fail, resulting in the growth of fracture zones. These phenomena of initiation and growth of fracture zones with fabric's extension are shown in Fig. 10 and Fig.11. The growth in fracture zones for loading along MD was slower as compared to that along CD. Since multiple fracture zones were developed in the fabric during its extension, the ones shown by the arrows in Fig. 10 and Fig. 11 are presented in Fig. 17 in terms of the normalized length of the fracture zone. The latter is introduced to quantify this process and is defined as a ratio of the length of fracture zone l_{fz} measured as the average distance between two sides of the zone along the loading direction (i.e. parallel to the main specimen's axis)to the current total length of fabric (L). . The fracture zone developed along MD after fabrics' extension of 50% and reached approximately half of the fabric's length at 200% extension. In contrast, for CD it started only after 180% extension, and the specimen of fabric failed at that fracture zone at fabric's extension of 200%. This shows that the development of fracture zone by the progressive failure of fibres was rapid for loading along CD and more protracted for MD. This phenomenon can be attributed to the preferential orientation of fibres along MD, i.e. in this case fibres, already more aligned along the loading direction (coinciding with MD), started participating in a load transfer while other fibres still re-oriented, resulting in more gradual damage evolution. Whereas, during loading in CD, most of the fibres reoriented along the loading direction and started participating in the load-bearing process practically at the same stage of the deformation process. Since the process of individual fibre failures responsible for damage evolution in the fabric

was more gradual along MD than CD, a longer tail in the force-extension curves was observed in the former case as shown in Fig. 11.

The model developed in this study is not only capable to predict the deformation and damage behaviour accurately in terms of anisotropy, nominal strength, force-extension behaviour and changes in network topology as a result of damage evolution but it also properly reflects the effect of grip constraints on the deformation behaviour of the fabric specimen (Fig. 10 and Fig. 11). The transverse strain in the fabric gradually increases from the grip on each end of the fabric to the region of maximum transverse strains in the middle. Such transverse strains in the fabric were significantly higher for MD, producing a visible necking effect in this case as compared to that in CD with negligibly small transverse strains at the initial stages of fabric's extension as shown in Fig. 10 and Fig. 11. However, after a certain level of fabric's extension along CD, significant transverse strains and, thus, necking was observed there (Fig. 11a). The reason for this different behaviour was the preferential orientation of fibres along MD in the fabric. In the model, for MD, visible necking in the fabric was observed similar to the experimental observations. Since fibres were taking the compressive load during fabric's extension along CD (shown in Fig. 16b) the necking in fabric was negligible even at higher levels of strains along that direction.

The damage evolution in fibrous networks can be characterised by a ratio $N_f / \bar{N}$, where N_f is the accumulated number of fibres failed at any particular level of fabric's extension and $\bar{N}$ is the total number of fibres failed during deformation and damage of the fabric up to its rupture. As the number of failed fibres depending upon failure locus can vary with variation in the ODF and positions of fibres within the fabric, therefore, the total number of fibres within the fabric specimen was not used as denominator in the introduced damage measure. Evolution of the damage parameter $N_f / \bar{N}$ with fabric's extension for both studied cases — MD and CD — is given in Fig. 18. It shows that the growth of damage caused by progressive fibre failure, a key feature of deformation

and damage of fibrous networks, was more gradual along MD than CD because of the reasons discussed above.

Another interesting observation was that the concentration of stresses at the edges of the bond points perpendicular to the direction of loading was very pronounced as compared to their other parts as shown in Fig. 19. Since fibres in thermally bonded nonwovens always fail at bond points, as mentioned in Section 2.2, the sharp stress concentration at bond points' edges is consistent with the experimental observations and various studies in the literature. However, the stress concentration at edges of bond points parallel to the loading direction was limited because these edges undergo compressive loading due to lateral contraction of the fabric as mentioned before (Fig. 10 and Fig. 11). Thus, the model developed in this study is also capable to simulate the stress distribution within bond points along with the areas of high stress concentration along its edges.

5. Conclusions

A micromechanical numerical model was developed in this study to simulate deformation as well as damage initiation and propagation in thermally bonded nonwoven fibrous networks. A subroutine, based on the parametric modelling technique, was used to develop this model. The fibres were introduced directly into the model according to their ODF obtained from the SEM images of the fabric using the image-analysis technique. This direct microstructure-based numerical approach maintains a relation between the microstructure of a nonwoven fibrous network and its deformation and damage behaviour. Moreover, this technique naturally introduced voids and gaps in fabric's microstructure, observed experimentally, into the model that cannot be achieved with a traditional continuous model.

All the parameters necessary for simulation of such a fibrous network, including the orientation distribution function for fibres, geometric properties, material properties, failure criteria as well as

the shape, size, dimensions and pattern of bond points were obtained with single-fibre and fabric experiments. The developed model reproduced mechanisms of fabric deformation and progressive damage observed in the uniaxial tensile tests. The simulation results were validated by means of comparison with these tests. The model was not only found to be in good agreement with experiments in terms of deformed shape of specimens and force-extension curves but also reproduced all the main features of fabric deformation and damage behaviour including:

- anisotropic behaviour;
- fibre re-orientation towards the loading direction that was more pronounced for CD than MD;
- failure of fibres on reaching their stress or strain thresholds leading to development of fracture zones;
- growth of the fracture zones due to progressive failure of fibres; the growth rate for fracture zones was higher for CD than MD;
- character of transverse strain including the grip effect;
- stress concentration at edges of the bond points.

The model developed with direct introduction of fibres according to their orientation distribution using the subroutine-based parametric modelling technique provides an opportunity for a direct study of the effects of variation in the fibrous network's geometry on its overall deformation and damage behaviour. Furthermore, the effect of variation in geometric properties of fibres and bond points can be studied using this model. This model not only captures the anisotropic force-extension behaviour of the material linked to its microstructure and material properties of constituent fibres but also provides an insight into specific features of deformation of fibres and the entire fabric as well as progressive damage mechanisms. Such capabilities of the model to capture all the main mechanisms and features of the fabric's response would underpin understanding the behaviour of the nonwoven fibrous networks and their structure-properties relationship.

Acknowledgement

We greatly acknowledge support by the Nonwovens Cooperative Research Centre of North Carolina State University, Raleigh, USA. FiberVisions®, USA generously provided the material for this study. We also acknowledge the use of Photrom (Fastcam SA3), borrowed from the EPSRC UK Engineering Instrument Pool.

References

Bais-Singh, S., Sherrill, B., Biggers, J.R., Bhuvenesh, Goswami, B. C., 1998. Finite element modeling of the nonuniform deformation of spun-bonded nonwovens. Textile Res. J. 68(5), 327-342.

Blacklock, M., Bale, H., Begley, M. R.,Cox, B.N., 2012. Generating virtual textile composite specimens using statistical data from micro-computed tomography: 1D tow representations for the binary model. J. Mech. Phys. Soilds 60, 451-470

Bronkhorst, C.A., 2003. Modelling paper as a two-dimensional elastic–plastic stochastic network. Int. J. Solids Struct. 40, 5441–5454.

Bhat, G. S., Jangala, P. K., Spruiell, J. E., 2004. Thermal bonding of polypropylene nonwovens: effect of bonding variables on the structure and properties of the fabric. J. Appl. Polymer Sci. 92, 3593-3600.

Chidambaram, A., Davis, H., Batra, S., 2000. Strength loss in thermally bonded polypropylene fibres. Inter Nonwovens J. 9, 27-35.

Demirci, E., Acar, M., Pourdeyhimi, B., Silberschmidt, V. V., 2011. Finite element modelling of thermally bonded bicomponent fibre nonwovens: tensile behaviour. Comput. Mater. Sci. 50, 1286-1291.

Demirci, E., Acar, M., Pourdeyhimi, B., Silberschmidt, V. V., 2012. Computation of mechanical anisotropy in thermally bonded component fibre nonwovens. Comput. Mater. Sci. 52, 157-163..

Farukh, F., Demirci, E., Sabuncuoglu, B., Acar, M., Pourdeyhimi, B., Silberschmidt, V. V., 2012a. Numerical modelling of damage initiation in low-density thermally bonded nonwovens. Comput. Mater. Sci. 64, 112-115.

Farukh, F., Demirci, E., Acar, M., Pourdeyhimi, B., Silberschmidt, V. V., 2012b. Meso-scale deformation and damage in thermally bonded nonwovens. J. Mater. Sci. 48, 2334-2345.

FiberVisions, USA, 2010. Manufacturer's Data Sheet.

Harrysson, A., Ristinmaa, M., 2008. Large strain elasto-plastic model of paper and corrugated board. Int. J. Solids and Struct. 45, 3334–3352.

Hou, X., Acar, M., Silberschmidt, V. V., 2009. 2D dinifte element analysis of thermally bonded nonwoven materials: continuous and discontinuous models. Comput. Mater. Sci. 46, 700-707.

Hou, X., Acar, M., Silberschmidt, V. V., 2011. Finite element simulation of low-density thermally bonded nonwoven materials:effect of orientation distribution function and arrangement of bond points. Comput. Mater. Sci. 50, 1292-1298.

Hou, X., Acar, M., Silberschmidt, V. V., 2011. Non-uniformity of deformation in low-density thermally bonded nonwoven material: effect of microstructure. J. Mater. Sci. 46, 307-315.

Isaksson, P., Hagglund, R., Gradin, P., 2004, Continuum damage mechanics applied to paper. Int. J. Solids Struct. 41, 4731-4755.

Isaksson, P., Hagglund, R., 2007. Analysis of the strain field in the vicinity of a crack-tip an in-plane isotropic paper material. Int. J. Solids Struct. 44, 659-671.

Isaksson, P., Hagglund, R., 2009. Structural effects on deformation and fracture of random fiber networks and consequences on continuum models. Int. J. Solids Struct. 46, 2320-2329.

Isaksson, P., Dumont, P.J.J., Roscoat, S. R. 2012. Crack growth in planar elastic fiber materials. Int. J. Soildds Struct. 49(13), 1900-1907.

Li, Z., Sun, B. Gu, B., 2010, FEM simulation of 3D angle-interlock woven composite under ballistic impact from unit cell approach. J. Mech. Phys. Soilds 49, 171-183

MSC. Marc, 2013. Volume A: Theory and user information. MSC.

Michielsen, S., Wang, X., 2002. Rapid morphology (property) changes at the bond periphery in thermal point-bonded. Nonwovens Int. J. 11(2), 35-38.

Ostoja-Starzewski, M., Stahl, D. C., 2000. Random fibre networks and special elastic orthotropy of paper. J. Elast. 60, 131-1349.

Petterson, D.R., 1959. On the Mechanics of Nonwoven Fabrics. PhD Thesis. Massachusetts Institute of Technology.

Parsons, E. M., King, M. J., Socrate, S., 2013. Modeling yarn slip in woven fabric at the continuum level: Simulations of ballistic impact. J. Mech. Phys. Soilds 61, 265-292

Russell, S. J., 2007. Handbook of nonwovens: Woodhead Publishing Limited.

Ridruejo, A., Gonza´lez, C., Llorca, J., 2010. Damage micromechanisms and notch sensitivity of glass-fibernon-noven felts:an experimental and numerical study. J. Mech. Phys. Solids 58,1628–1645.

Ridruejo, A., Gonza´lez, C., Llorca, J., 2011. Micromechanisms of deformation and fracture of polypropylene nonwoven fabrics. Int. J Solids Stuct. 48, 153-162.

Ridruejo, A., Gonza´lez, C., Llorca, J., 2012. A constitutive model for the in-plane mechanical behavior of nonwoven fabrics. 49 (17), 2215-2229.

Rinaldi, R.G., Blacklock, M., Bale, H., Begley, M. R.,Cox, B.N., 2012. Generating virtual textile composite specimens using statistical data from micro-computed tomography: 3D tow representations. J. Mech. Phys. Soilds 60, 1561-1581

Schulgasser, K., 1981. On the in-plane elastic constants of paper. Fibre Sci. Tech. 15, 257-270.

Silberstein, M. N., Pai, Chia-Ling, Rutledge, G. C., Boyce, M. C., 2012. Elastic–plastic behavior of non-woven fibrous mats. J. Mech. Phys. Solids 60(2), 295-318.

Simo, J.C., Hughes, T.J.R., 1998. Computational Inelasticity: Springer.

Sabuncuoglu, B., Acar, M., Silberschmidt, V. V., 2012. A parametric finite element analysis method for low-density thermally bonded nonwovens. Comput. Mater. Sci. 52, 164-170.

Sabuncuoglu, B., Acar, M., Silberschmidt, V. V., 2013, Parametric code for generation of finite-element model of nonwovens accounting for orientation distribution of fibres. Int. J. Numer. Meth. Engng., 94, 441–453.

Wang, X., Michielsen, S., 2001. Morphology gradients in thermally point-bonded polypropylene nonwovens. Textile Res. J., 7, 475-480.

Wang, X., Michielsen, S., 2002. Morphology gradients in thermally point-bonded poly(ethylene terephthalate) nonwovens. Textile Res. J. 72, 394-398.

Wilbrink, D.V., Beex, L.A.A., Peelings, R.H.J., 2013. A discrete network model for bond failure and frictional sliding in fibrous materials. Int. J Solids Stuct., 50, 1354-1363

Captions

Fig. 1. SEM images of 20 g/m2 PP fibre nonwoven

Fig. 2. Mechanical behaviour of PP fibre at various strain rates

Fig. 3. Orientation distribution function of fibres (90^o corresponds to MD whereas 0^o and 180^o correspond to CD)

Fig. 4. Force-elongation curves in tension at strain rate of 0.1 1/s along MD (a) and CD (b)

Fig. 5. Deformation and damage mechanisms in low-density thermally bonded nonwoven during tensile tests at 0% strain (a); 25% strain (b); 50 % strain (c); 80% strain (d). Loading direction was along MD and arrows indicate some fracture zones

Fig. 6. Effect of bonding on single-fibre's ultimate tensile stress (a) and strain (b)

Fig. 7. Paramters of pattern of modelled fabric

Fig.8. Stochasticity in material properties implemented into FE model: (a) stress-strain curves; (b) critical values of stress and strain

Fig. 9. (a) FE model showing stochasticity in material properties and fibres' orientation distribution; (b) zoomed view of bond point showing truss elements connected to shell elements

Fig. 10. (a) Experimental results for fabric subjected to uniaxial tension along MD to various extensions: (i) 25%; (ii) 50%; (iii) 75%; (iv) 100%; (v) 150%; (vi) 190%; (b) corresponding FE model results for equivalent (von Mises) stresses in (MPa)

Fig. 11. (a) Experimental results for fabric subjected to uniaxial tension along CD to various extensions: (i) 25%; (ii) 50%; (iii) 75%; (iv) 100%; (v) 150%; (vi) 190%; (b) corresponding FE model results for equivalent (von Mises) stresses in (MPa)

Fig. 12. Calculated responses to uniaxial tensile test for MD (a) and CD (b) (Shaded area represents scatter in experimental results)

Fig. 13. Flow chart on implementation of stochasticity in FE model

Fig. 14. Distribution of normalised strains for fibres for various values of fabric strain deformed along MD (a) and CD (b)

Fig. 15. Distribution of stresses for fibres for various values of fabric strain deformed along MD (a) and CD (b)

Fig. 16. Minimum and maximum values of stress in fibres for various values of strain in fabric deformed along MD (a) and CD (b)

Fig. 17. Growth in fracture zone with fabric's extension

Fig. 18. Evolution of damage parameter with fabric's deformation

Fig. 19. Equivalent von Mises (MPa) stress concentration at edges of bond points (loading direction was along MD)

Tables

Table 1. Properties of polypropylene fibre (as extracted from nonwovens)

ρ_f (g/cm^3)	E_f (MPa)	ν_f	σ_y (MPa)
0.89	350±42	0.42 (FiberVisions, 2010)	75±9

Table 2. Number of elements for MD and CD models

	Shell (element type 139)	Truss (element type 9)
MD	11420	2285
CD	9750	2067

Table 3. Parameters of fabric (see Fig. 7)

	Parameter	Magnitude
Fabric	A_{Fabric} (W x L) (mm x mm)	MD: 10 x 16.5 CD : 16.5 x 10
	ρ_{Fabric} (kg/m^2)	20 x 10^{-3}
Parameters of bond points pattern	A (mm)	1.0668
	B (mm)	0.5588
	C (mm)	0.7
	D (mm)	1.8
	E (mm)	0.2
Fibres	a_{Fibre} (mm^2)	0.0003
	L_{Fibre} (mm)	38.1
	ρ_{Fibre} (kg/m^3)	0.89 x 10^3
Model coefficient	k	1

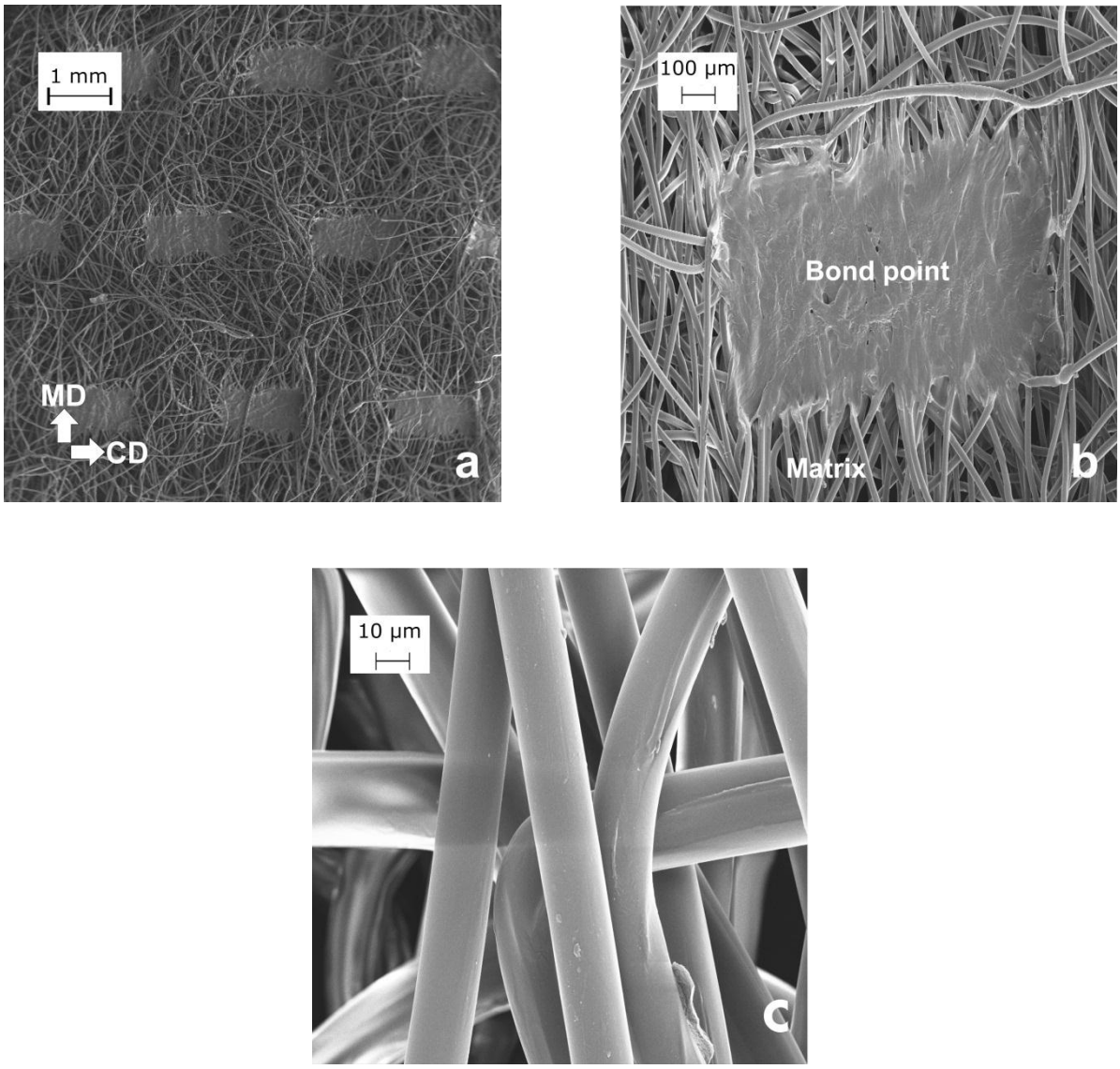

Fig. 1. SEM images of 20 g/m2 PP fibre nonwoven

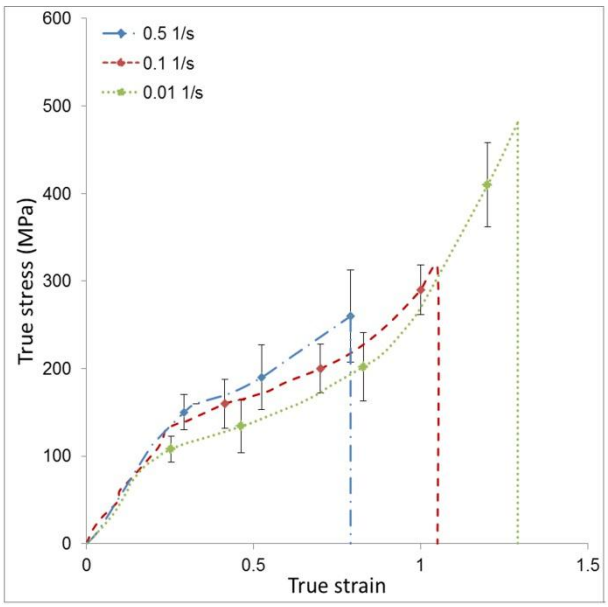

Fig. 2. Mechanical behaviour of PP fibre at various strain rates

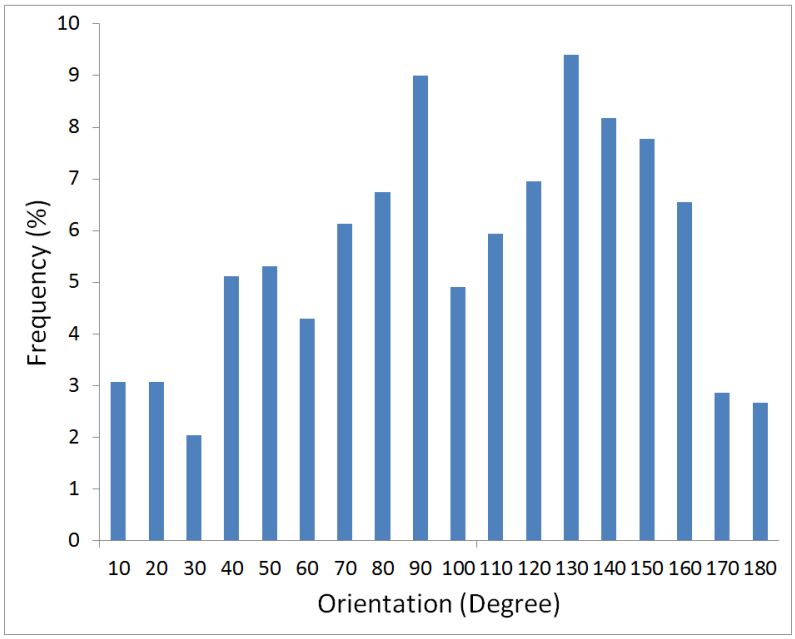

Fig. 3. Orientation distribution function of fibres (90o corresponds to MD whereas 0o and 180o correspond to CD)

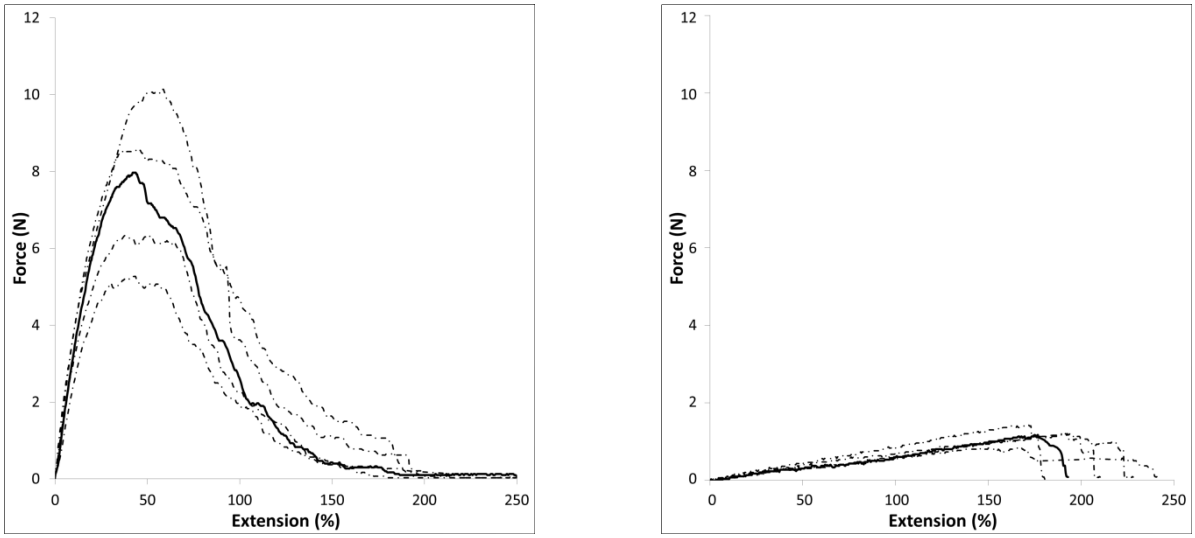

Fig. 4. Force-elongation curves in tension at strain rate of 0.1 1/s along MD (a) and CD (b)

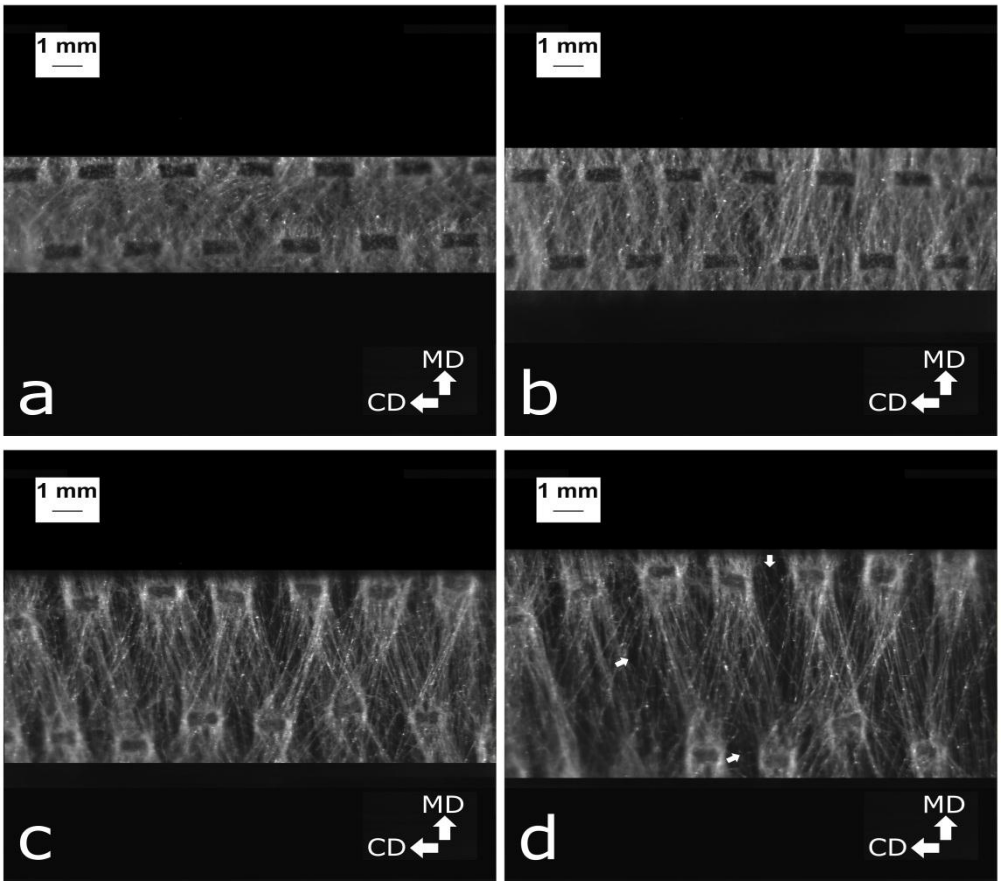

Fig. 5. Deformation and damage mechanisms in low-density thermally bonded nonwoven during tensile tests at 0% strain (a); 25% strain (b); 50 % strain (c); 80% strain (d). Loading direction was along MD and arrows indicate some fracture zones

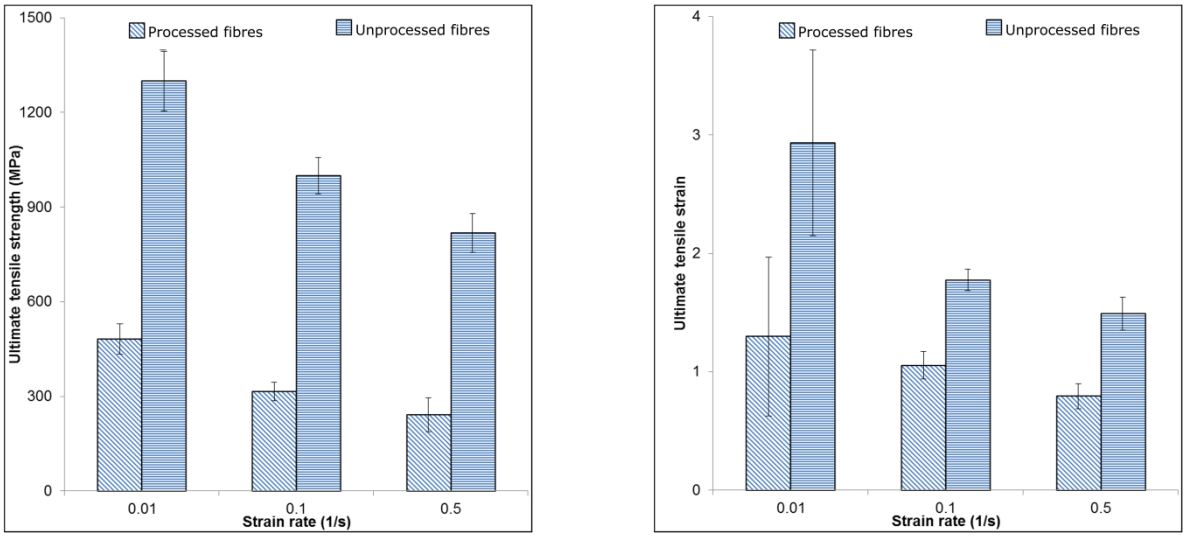

(a) (b)

Fig. 6. Effect of bonding on single-fibre's ultimate tensile stress (a) and strain(b)

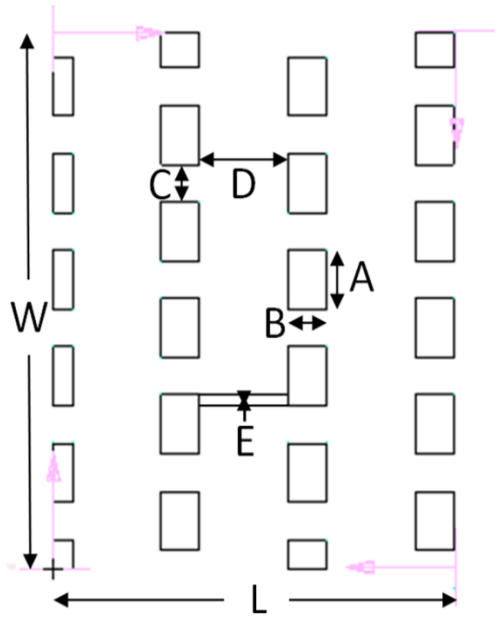

Fig. 7. Parameters of pattern of modelled fabric

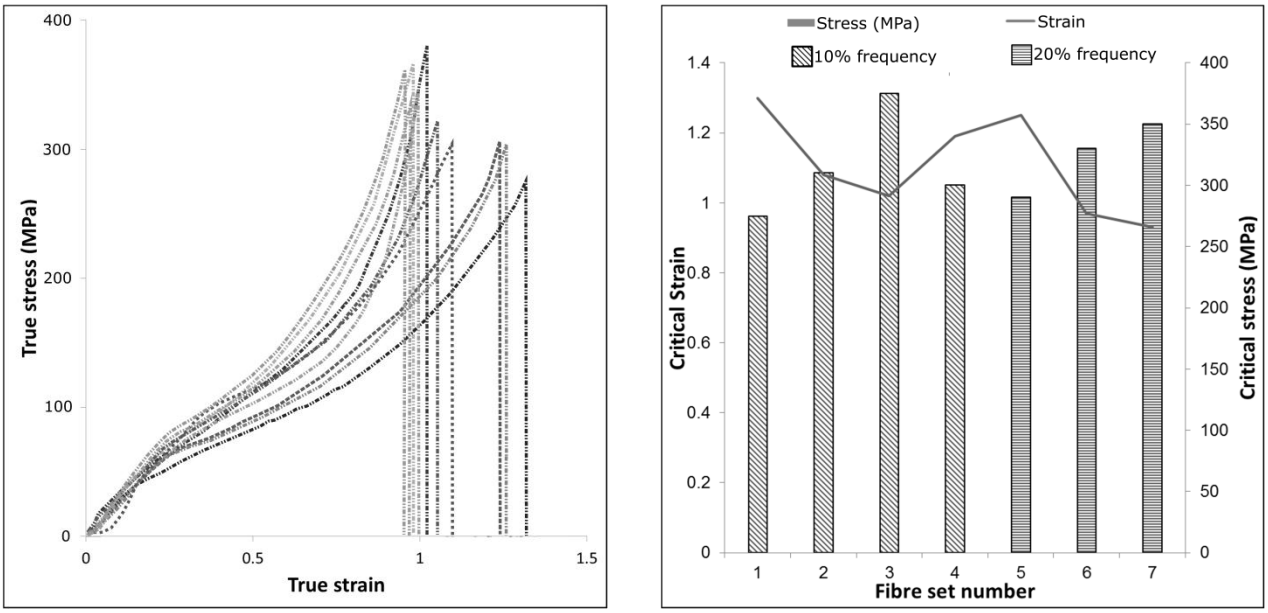

(a) (b)

Fig. 8. Stochasticity in material properties implemented into FE model: (a) stress-strain curves; (b) critical values of stress and strain

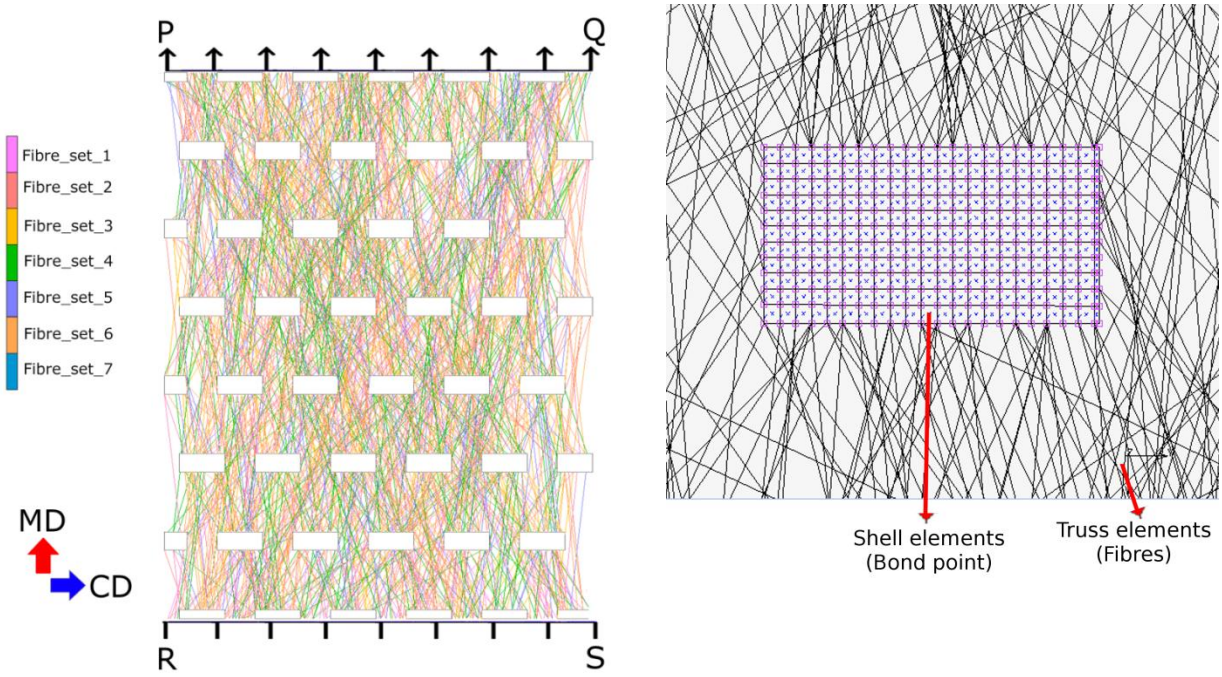

Fig. 9. (a) FE model showing stochasticity in material properties and fibres' orientation distribution; (b) zoomed view of bond point showing truss elements connected to shell elements

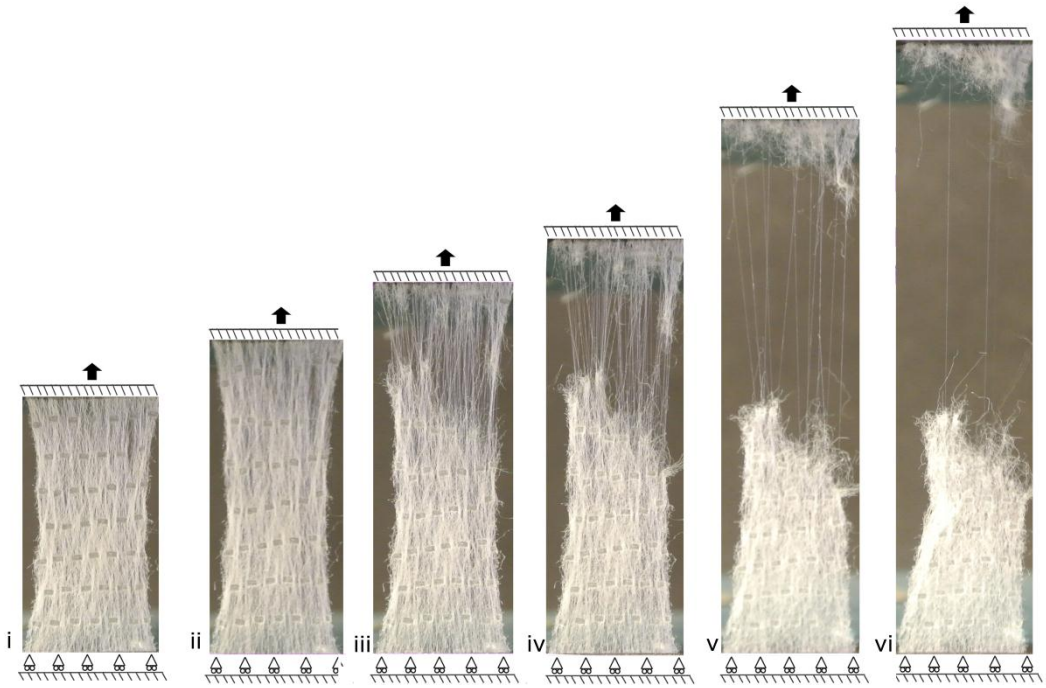

(a)

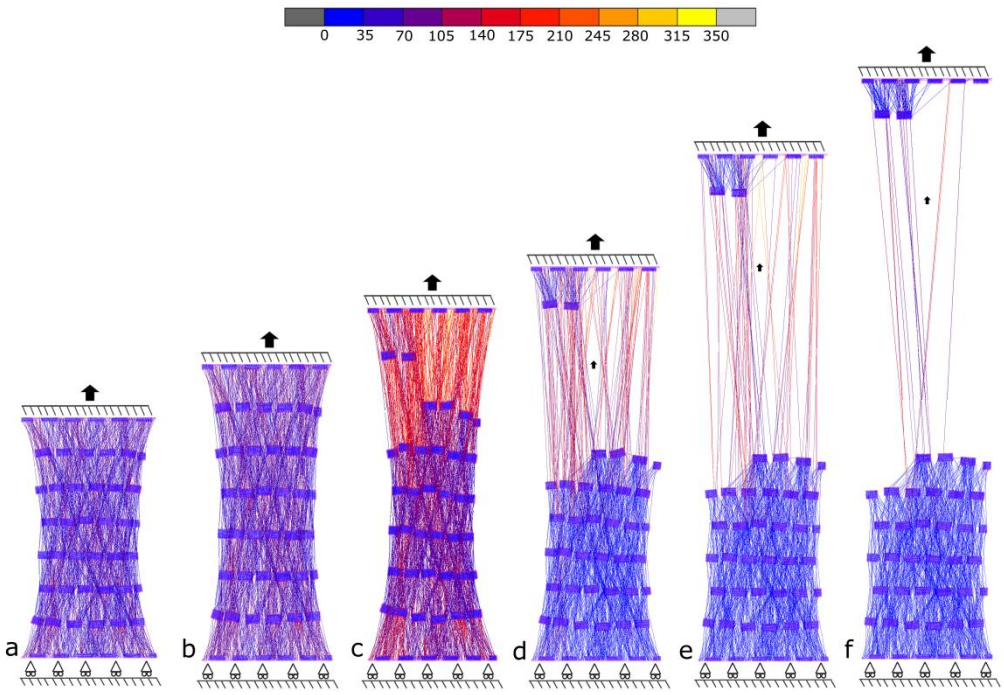

(b)

Fig. 10. (a) Experimental results for fabric subjected to uniaxial tension along MD to various extensions: (i) 25%; (ii) 50%; (iii) 75%; (iv) 100%; (v) 150%; (vi) 190%; (b) corresponding FE model results for equivalent (von Mises) stresses in (MPa)

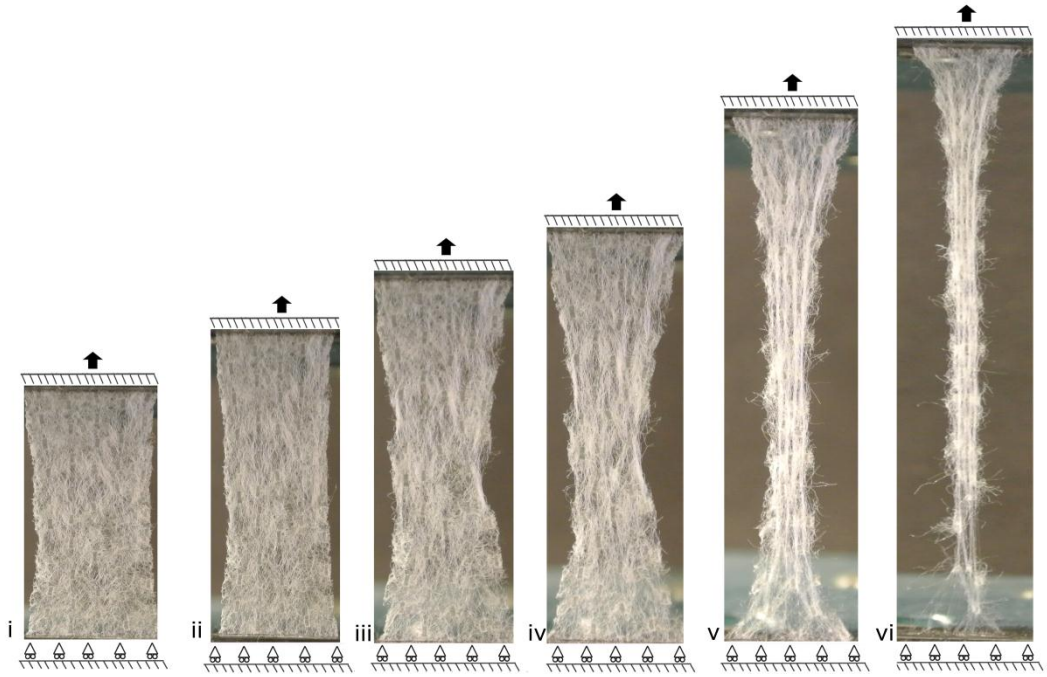

(a)

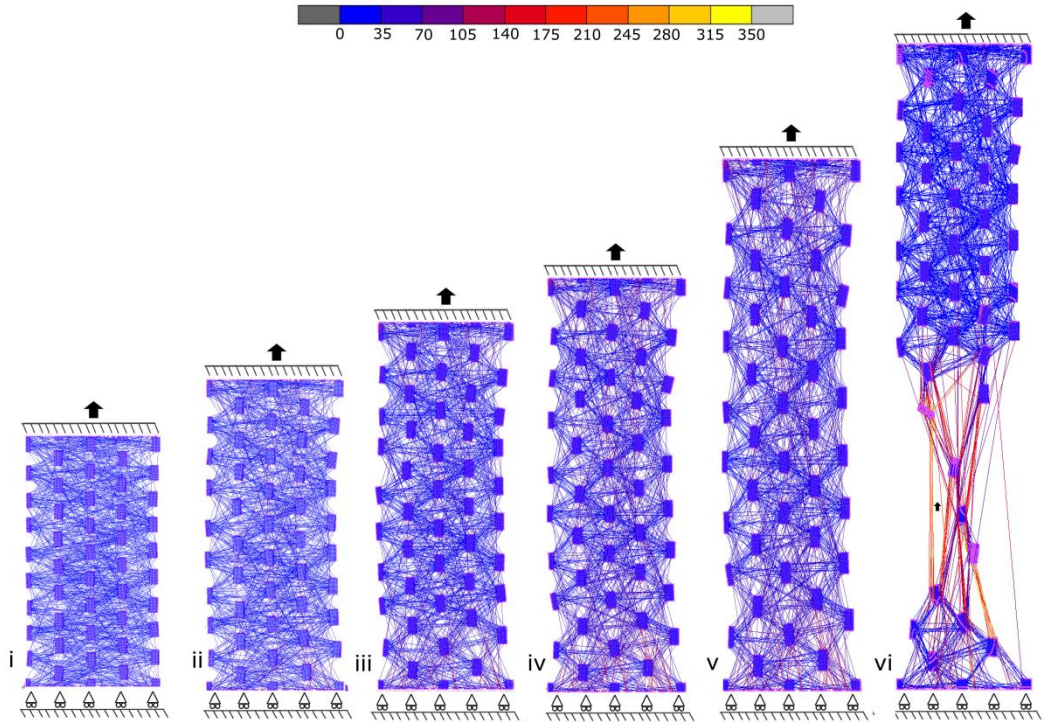

(b)

Fig. 11. (a) Experimental results for fabric subjected to uniaxial tension along CD to various extensions: (i) 25%; (ii) 50%; (iii) 75%; (iv) 100%; (v) 150%; (vi) 190%; (b) corresponding FE model results for equivalent (von Mises) stresses in (MPa)

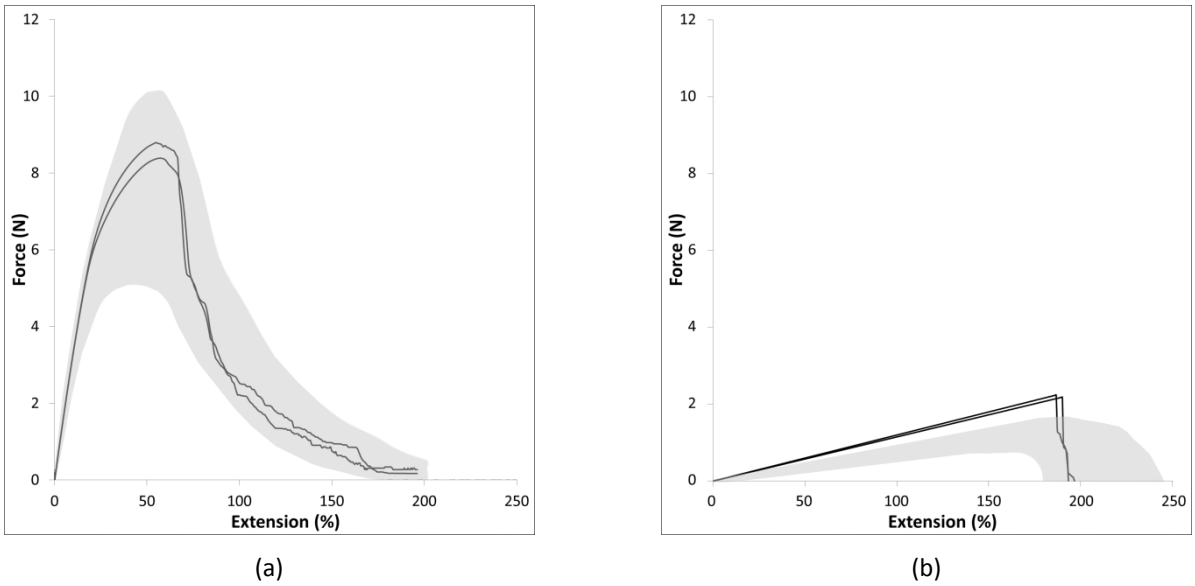

Fig. 12. Calculated responses to uniaxial tensile test for MD (a) and CD (b) (Shaded area represents scatter in experimental results)

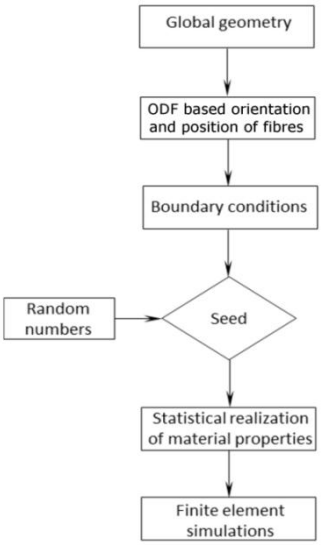

Fig. 13. Flow chart on implementation of stochasticity in FE model

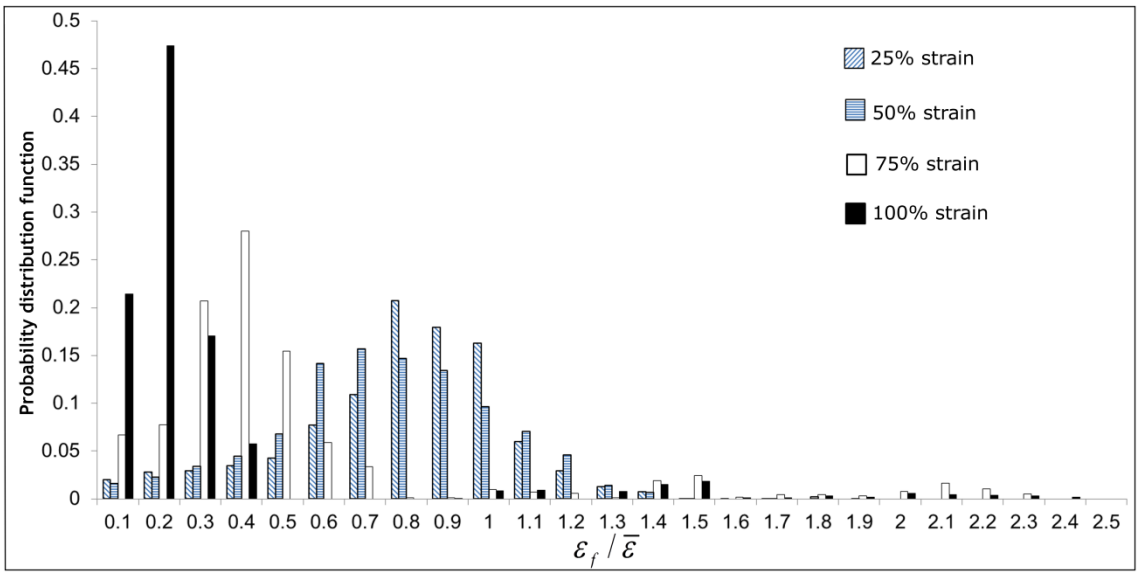

(a)

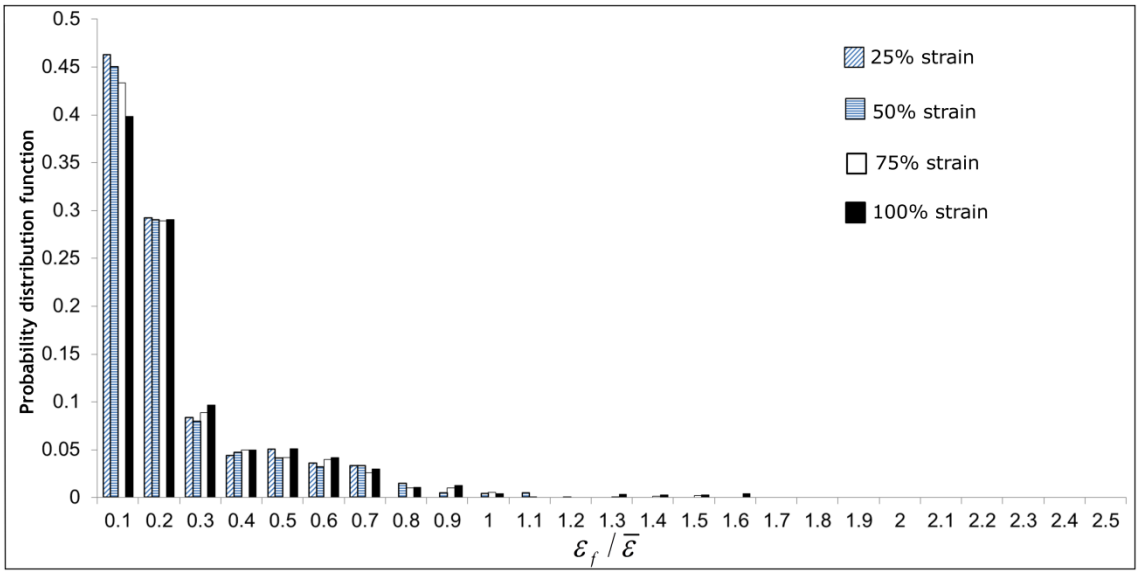

(b)

Fig. 14. Distribution of normalised strains for fibres for various values of fabric strain deformed along MD (a) and CD (b)

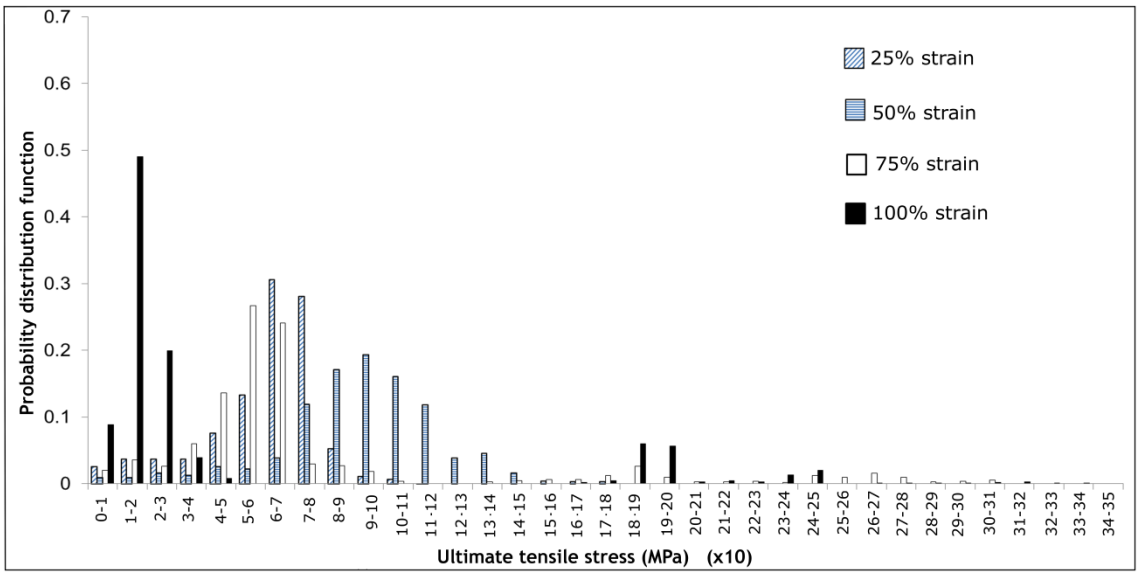

(a)

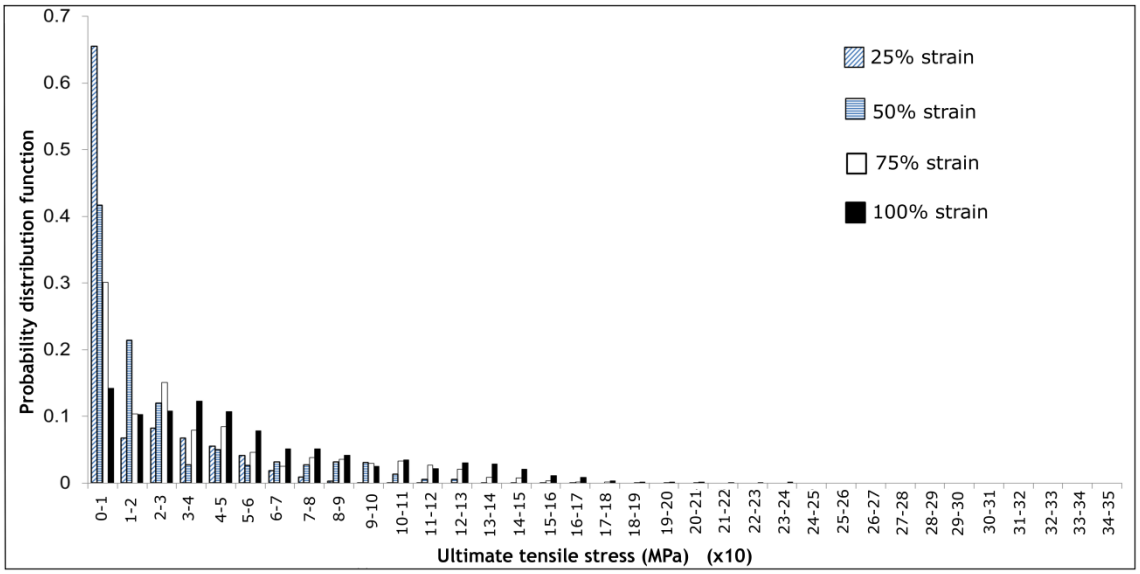

(b)

Fig. 15. Distribution of stresses for fibres for various values of fabric strain deformed along MD (a) and CD (b)

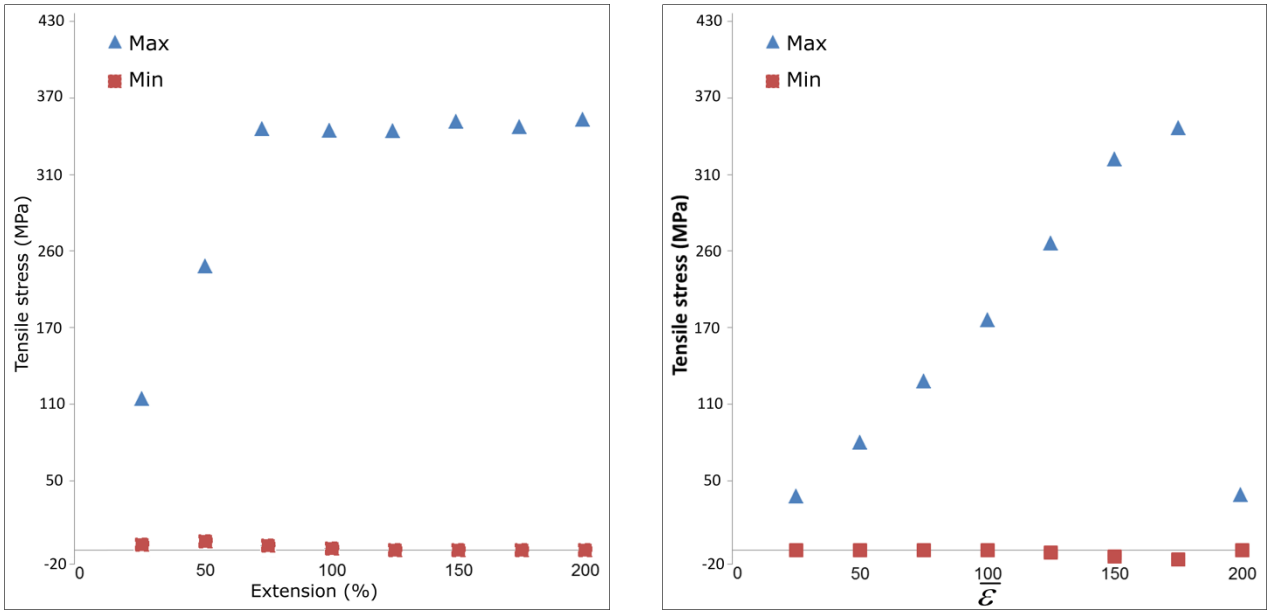

(a) (b)

Fig. 16. Minimum and maximum values of stress in fibres for various values of strain in fabric deformed along MD (a) and CD (b)

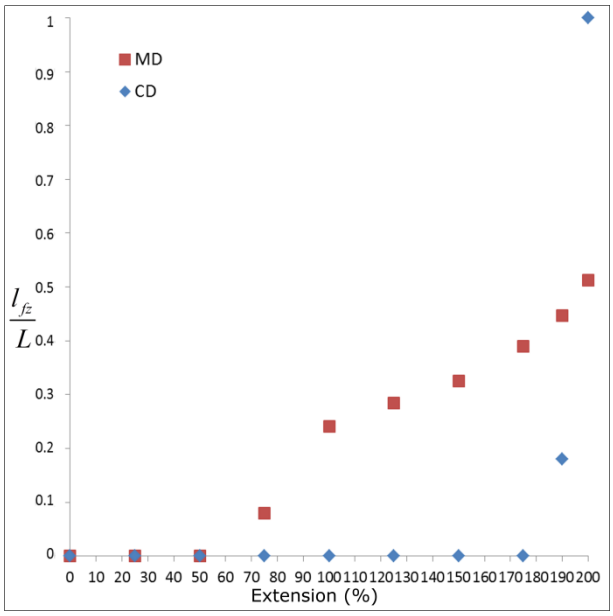

Fig. 17. Growth in fracture zone with fabric's strain

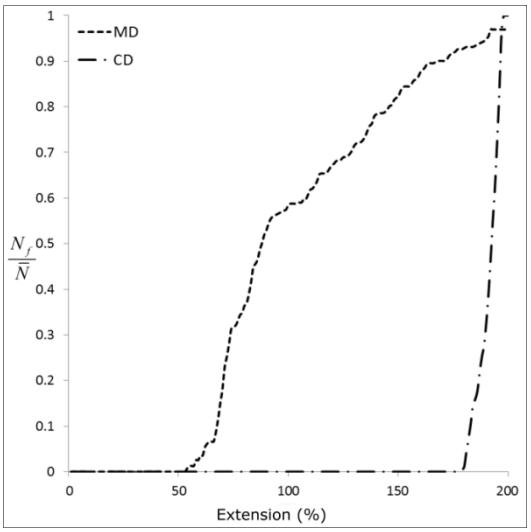

Fig. 18. Evolution of damage parameter with fabric's deformation

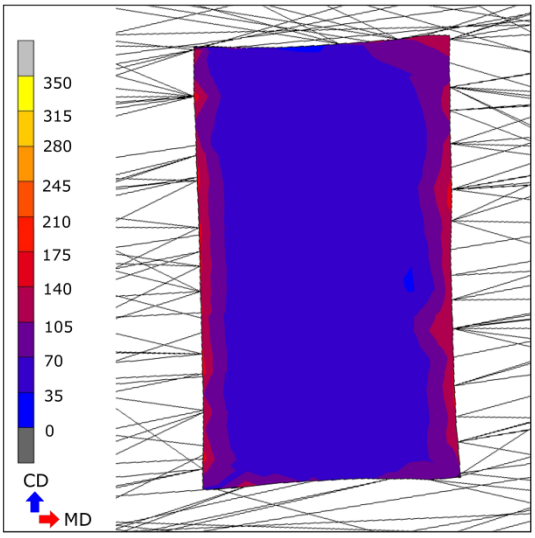

Fig. 19. Equivalent von Mises (MPa) stress concentration at edges of bond points (loading direction was along MD)